

Communication

Modelling and Design of a Dual Depletion PIN Photodiode as Temperature Sensor

Ricardo A. Marques Lameirinhas ^{1,2,*} , João Paulo N. Torres ^{2,3}  and Catarina P. Correia V. Bernardo ^{1,2} ¹ Department of Electrical and Computer Engineering, Instituto Superior Técnico, 1049-001 Lisbon, Portugal² Instituto de Telecomunicações, 1049-001 Lisbon, Portugal; joaotorres@ist.utl.pt³ Academia Militar/CINAMIL, Av. Conde Castro Guimarães, 2720-113 Amadora, Portugal

* Correspondence: ricardo.lameirinhas@tecnico.ulisboa.pt

Abstract: Nowadays, optical systems play an important role in communications. Dual depletion PIN photodiodes are common devices that can operate in different optical bands, depending on the chosen semiconductors. However, since semiconductor properties vary with the surrounding conditions, some optical devices/systems can act as sensors. In this research work, a numerical model is implemented to analyze the frequency response of this kind of structure. It considers both transit time and capacitive effects, and can be applied to compute photodiode frequency response under nonuniform illumination. The InP-In_{0.53}Ga_{0.47}As photodiode is usually used to convert optical into electrical power at wavelengths around 1300 nm (O-band). This model is implemented considering an input frequency variation of up to 100 GHz. The focus of this research work was essentially the determination of the device's bandwidth from the computed spectra. This was performed at three different temperatures: 275 K, 300 K, and 325 K. The aim of this research work was to analyze if a InP-In_{0.53}Ga_{0.47}As photodiode can act as a temperature sensor, to detect temperature variations. Furthermore, the device dimensions were optimized, to obtain a temperature sensor. The optimized device, for a 6 V applied voltage and an active area of 500 μm², had a total length of 2.536 μm, in which 53.95% corresponded to the absorption region. In these conditions, if the temperature increases 25 K from the room temperature, one should expect a bandwidth increase of 8.374 GHz, and if it decreases 25 K from that reference, the bandwidth should reduce by 3.620 GHz. This temperature sensor could be incorporated in common InP photonic integrated circuits, which are commonly used in telecommunications.

Keywords: InP-In_{0.53}Ga_{0.47}As photodiode; optical sensors; optics; optoelectronics; photodiodes; PIN structures



Citation: Marques Lameirinhas, R.A.; N. Torres, J.P.; P. Correia V. Bernardo, C. Modelling and Design of a Dual Depletion PIN Photodiode as Temperature Sensor. *Sensors* **2023**, *23*, 4599. <https://doi.org/10.3390/s23104599>

Academic Editor: Gabriele Bolognini

Received: 13 April 2023

Revised: 28 April 2023

Accepted: 6 May 2023

Published: 9 May 2023



Copyright: © 2023 by the authors. Licensee MDPI, Basel, Switzerland. This article is an open access article distributed under the terms and conditions of the Creative Commons Attribution (CC BY) license (<https://creativecommons.org/licenses/by/4.0/>).

1. Introduction

Photodiodes are important components in optical systems. They allow us to convert optical into electrical power and, consequently, the transition between the two domains allow us to consider both domains' advantages when designing a communication system. A commonly analyzed structure is the PIN type, mainly due to its good frequency response, great sensitivity, and excellent signal-to-noise ratio [1–7].

Other figures of merit are also important to consider. The most important figures of merit related to photodetection are responsivity and photoconductive gain; efficiency and quantum efficiency; spectral selectivity and ultraviolet-to-visible rejection ratio; detectivity and noise-equivalent power; and bandwidth and time response. Different photodetectors can be compared using quantitative results from this list. In optical communications, bandwidth and quantum efficiency are important figures of merit, mainly because bandwidth is related to the system bitrate and the quantum efficiency is related to the photodetector sensitivity [1,2,5].

Furthermore, a given photodetector might act as a sensor, due to the fact that the material properties must change with certain stimuli [7]. This might lead to changes in

the figure of merit values. Thus, it is possible to optimize the function of a photodiode to monitor certain stimuli, adding further capabilities to optical communication systems.

The use of these periodic structures as sensors has been studied, since their manufacture and reproducibility seems not to be a difficult issue for specialized companies [1,5,8]. The main focus is on the optimization process, since the design goals are different. The research problem is now more complex. Besides the optimization of the device dimensions to reach a certain figure of merit and client specifications, to design a sensor, it is necessary to analyze it with different stimuli and verify the variations of the device response.

In the case of semiconductors materials, some material dependencies are commonly studied, such as the variation of their properties with temperature [7]. InP-In_{0.53}Ga_{0.47}As photodetectors work at 1300 nm, with tens or hundreds of GHz of bandwidth [5,8–10]. This temperature sensor could be incorporated into common InP photonic integrated circuits, which have an excellent cost–performance relation. InP photonic integrated circuits are commonly used in telecommunications. The main aim of this research work was to optimize a dual depletion InP-In_{0.53}Ga_{0.47}As PIN photodiode as a temperature sensor, exploring its bandwidth variations. In order to achieve this, a model based on continuity equations was implemented, exploiting matrix relations to determine the frequency response of this type of device.

2. Methodology

2.1. Structural Analysis

The analyzed structure was a dual depletion PIN photodiode, as illustrated in Figure 1. It is composed of two InP contacts, one n+ where the light flux is incident on, and another p+ on the other side. Between them, there are two regions. After the n+ contact, there is a drift InP region (D) and an absorption In_{0.53}Ga_{0.47}As region (A). The contact dimensions and interfaces are neglected, and the devices have a total l_t length, divided into l_d and l_a for the drift and absorption region lengths, respectively. In addition, p_a is defined as the absorption layer thickness percentage of the total device, l_a/l_t . These semiconductors were chosen in order to have a high absorption between 1.0 μm and 1.6 μm , namely at 1.3 μm in the center of the original optical band (O-band). Both semiconductors were lattice matched [1,4,7,8,10].

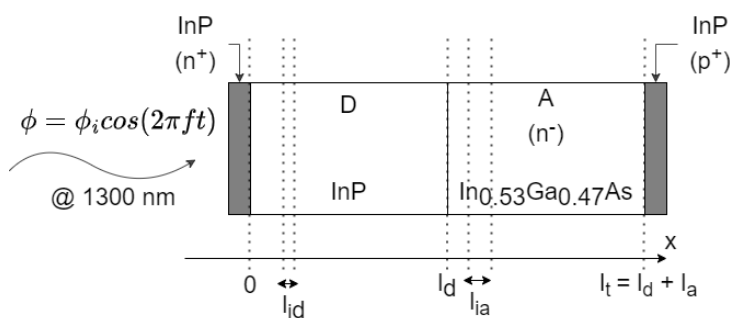


Figure 1. InP-In_{0.53}Ga_{0.47}As PIN photodiode schematic.

Different responses can be obtained if radiation is incident on either side; for instance, on the p contact side or directly on the intrinsic region.

A model based on the capacitive and transit time effects of a dual depletion PIN photodiode was implemented, which was previously proposed and validated in [1]. The dual depletion PIN photodiode capacitive effects are mainly due to its junction capacitance and certain other parasitic effects, such as those related to the pads and packages. On the other hand, the transit time effects are associated with the electron and hole transport in the drift and absorption regions, due to the electric field. Consequently, they are related to the carrier's drift velocity and the length of both regions [1,8–10].

Thus, both effects should be analyzed in order to evaluate a device's performance. It is known that the longer the device length, the shorter the transit time will be. On the other

hand, by increasing the device length, the capacitance will increase. For this reason, the photoconversion of a device is dependent on the device geometry [1,8–10].

2.2. Proposed Method

Based on continuity equations, it is possible to establish matrix relations to obtain the frequency response of this kind of device. The analytical solution of these equations can be obtained for constant electrical fields [1]. However, the used methodology decomposes the regions into several layers of a constant electric field, but this can change among them. Analytical solutions can be obtained in each layer, and by combining the solution coefficients, it is possible to compute the frequency response. Consequently, the higher the number of layers, the higher the accuracy of the numerical method.

In the analyzed PIN structure, the electric field is constant in the drift region and it varies linearly in the absorption region. In the frequency domain expressions, (1) and (2) are used to compute the current of the electron, J_{in} , and holes, J_{ip} , respectively, in the i -th layer of the constant electric field, considering the respective drift velocities v_{in} and v_{ip} [1].

$$\frac{j\omega}{v_{in}} J_{in}(x, \omega) = \frac{d J_{in}(x, \omega)}{d x} + G_i(x, \omega) \quad (1)$$

$$\frac{j\omega}{v_{ip}} J_{ip}(x, \omega) = \frac{d J_{ip}(x, \omega)}{d x} + G_i(x, \omega) \quad (2)$$

The PIN structure was illuminated on the $n+$ side contact using a sinusoidal optical flux of amplitude ϕ_i and frequency ω , leading to an electron–hole pair generation rate $G_i(x, \omega)$, defined in expression (3) [1]. This had a null value in the drift region and was dependent on the absorption coefficient α and on the electron charge module q in the absorption region. The optical stimuli was absorbed in this region. The x coordinate was substituted by the value of x_i associated with each layer. Once again, the accuracy of the numerical method was increased by increasing the number of layers.

In contrast to the previous study [1], where this method was proposed, in this article, the null branch of $G_i(x, \omega)$ was not used. To improve the method's accuracy, both drift and absorption regions were characterized using the complex electrical permittivity or equivalently using the complex refractive index. Consequently, the drift region was characterized identically to the absorption region, but with different values.

$$G_i(x, \omega) = \begin{cases} 0 & (0 \leq x \leq l_d) \\ q \alpha \phi_i e^{-\alpha(x-l_d)} & (l_d \leq x \leq l_d + l_a) \end{cases} \quad (3)$$

The linear coefficients of \mathbf{T}_i , \mathbf{S}_i , \mathbf{R}_i , and D_i for each i -th layer were obtained by solving the continuity equations [1].

Expression (4) relates \mathbf{T}_i and \mathbf{S}_i coefficients, defined in expressions (5) and (6), with the electron and hole current densities. \mathbf{T}_i are named as current transfer matrices and \mathbf{S}_i are the current contribution from the optical sources.

$$\begin{bmatrix} J_p(x_i) \\ J_n(x_i) \end{bmatrix} = \mathbf{T}_i \begin{bmatrix} J_p(x_{i-1}) \\ J_n(x_{i-1}) \end{bmatrix} + \mathbf{S}_i \quad (4)$$

$$\mathbf{T}_i = \begin{bmatrix} T_{ipp} & T_{ipn} \\ T_{inp} & T_{inn} \end{bmatrix} \quad (5)$$

$$\mathbf{S}_i = \begin{bmatrix} S_{ip} \\ S_{in} \end{bmatrix} \quad (6)$$

On the other hand, \mathbf{R}_i and D_i are settled in expression (7), where $p_i(\omega)$ is the partial electrode current [1].

On the other hand, \mathbf{R}_i and D_i are settled in expression (7), where $p_i(\omega)$ is the partial electrode current. D_i is scalar and it is related to optical sources, whereas \mathbf{R}_i is defined in (8) and it relates the left-hand terminal currents and $p_i(\omega)$.

$$p_i(\omega) = \int_{l_i} [J_n(x, \omega) + J_p(x, \omega)] dx = \mathbf{S}_i^T \begin{bmatrix} J_p(x_{i-1}) \\ J_n(x_{i-1}) \end{bmatrix} + D_i \quad (7)$$

$$\mathbf{R}_i = \begin{bmatrix} R_{ip} \\ R_{in} \end{bmatrix} \quad (8)$$

The multilayer structure coefficients were obtained by recursively computing the expression set (9). These operations allowed the union of the i -th and the $(i+1)$ -th layer, its coefficients being defined as $(i+1, i)$. At the end of this computation, the coefficients were representative of the entire structure's performance.

$$\begin{cases} \mathbf{T}_{i+1,i} = \mathbf{T}_{i+1} \mathbf{T}_i \\ \mathbf{S}_{i+1,i} = \mathbf{S}_{i+1} + \mathbf{T}_{i+1} \mathbf{S}_i \\ \mathbf{R}_{i+1,i}^T = \mathbf{R}_{i+1}^T \mathbf{T}_i + \mathbf{R}_i^T \\ D_{i+1,i} = \mathbf{R}_{i+1}^T \mathbf{S}_i + D_{i+1} + D_i \end{cases} \quad (9)$$

The frequency response of the photogenerated current $I(\omega)$ is defined by expressions (10) and (11), related to the whole structure coefficients.

$$I(\omega) = \frac{\delta(\omega)}{l_a + l_d} \quad (10)$$

$$\delta(\omega) = D - \frac{R_n S_n}{T_{nn}} \quad (11)$$

The coefficients \mathbf{T}_i and \mathbf{S}_i were deduced in [1] as presented in expressions (12) and (13), as well as the coefficients of \mathbf{R}_i and D_i in expressions (14) and (15). $f(\theta) = \frac{1-e^{-\theta}}{\theta}$ is denoted as an auxiliary function, to simplify the expressions' presentation, as well as $\tau_{in} = \frac{l_i}{v_{in}}$ and $\tau_{ip} = \frac{l_i}{v_{ip}}$ as the electron and hole transit time in the i -th layer, respectively.

$$\mathbf{T}_i = \begin{bmatrix} e^{-j\omega\tau_{ip}} & 0 \\ 0 & e^{j\omega\tau_{in}} \end{bmatrix} \quad (12)$$

$$\mathbf{S}_i = q\alpha\phi_i l_i e^{-\alpha x_i} \begin{bmatrix} f(j\omega\tau_{ip} - \alpha l_i) \\ -f(-j\omega\tau_{in} - \alpha l_i) \end{bmatrix} \quad (13)$$

$$\mathbf{R}_i = l_i \begin{bmatrix} f(j\omega\tau_{ip}) \\ f(-j\omega\tau_{in}) \end{bmatrix} \quad (14)$$

$$D_i = q\alpha\phi_i l_i^2 e^{\alpha(l_i - x_i)} \times \left(\frac{f(\alpha l_i) - f(-j\omega\tau_{in})}{\alpha l_i + j\omega\tau_{in}} - \frac{f(\alpha l_i) - f(j\omega\tau_{ip})}{\alpha l_i - j\omega\tau_{ip}} \right) \quad (15)$$

The implemented model is a more general approach in comparison with the one presented in [1]. In this research work, the model was implemented in Python. In this case, the drift and absorption layers were treated equally. In [1], the coefficients for the drift layers were different from the ones for the absorption layer, due to the fact that the absorption coefficient and the carrier velocities must be null. In this article, general expressions are deduced, and every i -th layer (in drift and absorption regions) is considered. This was used to analyze a device with a drift and an absorption region; however, following this novel approach, a N-region structure might be considered, even though it does not

characterize the layers as drift and absorption, and only characterizing with the properties of the medium.

In addition, the aim in [1] was to obtain the frequency response of InP-In_{0.53}Ga_{0.47}As photodiodes, to be used in communication systems, whereas in this article the aim was to investigate the use of these photodiodes as temperature sensors, and optimizing their dimensions for that purpose.

2.3. Semiconductor Properties

The semiconductor models for the InP drift region and for the In_{0.53}Ga_{0.47}As absorption region at 300 K were obtained from [11,12], respectively. In Table 1 are the parameters used from these references. Moreover, there are the parameters at two other temperatures used in the temperature sensor simulation. The semiconductor property models were introduced into the general model, in order to consider temperature as an initial condition.

Table 1. Material parameters at different temperatures (* 1×10^{-100} was used to emulate zero, in order to test the generalization of the matrix formalism).

Parameters	Units	Temperature					
		300 K		275 K		325 K	
		In _{0.53} Ga _{0.47} As	InP	In _{0.53} Ga _{0.47} As	InP	In _{0.53} Ga _{0.47} As	InP
Absorption Coefficient ($\alpha@1.3 \mu\text{m}$)	m^{-1}	1.15×10^6	*	1.13×10^6	*	1.12×10^6	*
Electron Saturation Velocity (v_{ni})	m/s	6×10^4	8.11×10^4	6.2425×10^4	8.11×10^4	5.9775×10^4	8.11×10^4
Hole Saturation Velocity (v_{pl})	m/s	4.8×10^4	8.11×10^4	5.1325×10^4	8.11×10^4	4.8675×10^4	8.11×10^4
Electron Mobility (μ_n)	$\text{m}^2\text{V}^{-1}\text{s}^{-1}$	1.05	*	1.15	*	0.969	*
Hole Mobility (μ_p)	$\text{m}^2\text{V}^{-1}\text{s}^{-1}$	0.042	*	0.046	*	0.038	*
Electric Permittivity (ϵ)	F/m	$14.1\epsilon_0$	$12.56\epsilon_0$	$14.1\epsilon_0$	$12.56\epsilon_0$	$14.1\epsilon_0$	$12.56\epsilon_0$

The parameter variations with temperature are reported in [7,13,14]. The used carrier velocity models are also dependent on the applied electric field (applied voltage) and on the residual donor concentration in the absorption region [1].

A small signal equivalent circuit was used to convert the optical excitation into an electrical current, as illustrated in [1]. In this computation, an infinity leakage resistance was assumed, in order to obtain a reasonable transfer function. Expression (16) was deduced from the equivalent circuit, relating the output current I_0 as a function of the optical excitation, $I_0 = H \times I$, for each working frequency [1,2].

$$H = \frac{1}{-\omega^2 R_L R_s C_p C_1 + j\omega(C_1(R_L + R_s) + R_L C_p) + 1} \quad (16)$$

Moreover, similar to what was reported in [1], a donor concentration of $N = 10 \times 10^{21} \text{ m}^{-3}$, a parasitic capacitance of $13 \times 10^{-15} \text{ F}$, and a load resistance of 50Ω were assumed.

In this research work, the number of absorption layers was set to 40 and there was only one drift layer. However, the method was implemented considering them as variables. The variation in the drift layer number may be useful if the drift region is absorption, which was not the case.

3. Method Validation

Before optimizing the frequency response of the dual depletion InGaAs/InP PIN photodiode, the implemented approach was validated with the prior one, confirming that its execution was correct.

Thus, for $l_t = 3 \mu\text{m}$ and a 10 V applied voltage, the obtained frequency response is presented in Figure 2, for three different values of p_a and considering an active area of $500 \mu\text{m}^2$. In the design stage, by sweeping the absorption layer thickness percentage it was possible to tune the device's optical response, namely its bandwidth. In these conditions,

it was also noticeable that this thickness variation could lead to significant fluctuations in the response at high frequencies. However, these devices in these conditions have a low-pass characteristic.

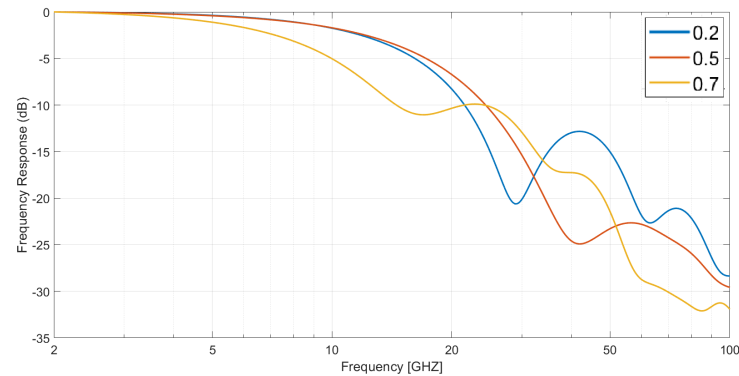


Figure 2. Frequency response of a dual depletion $\text{In}_{0.53}\text{Ga}_{0.47}\text{As}$ PIN photodiode with an active area of $500 \mu\text{m}^2$ and a total length of $3 \mu\text{m}$, working with a 10 V applied voltage, as a function of its absorption layer percentage at room temperature.

On the other hand, keeping the absorption layer percentage at $0.5 = 50\%$, but varying its thickness and the total one, it was concluded that the lower the total length, the better the response seemed to be, since it was smoother and it had no peaks in the analyzed frequency range. In Figure 3, these results are shown, assuming a 10 V applied voltage.

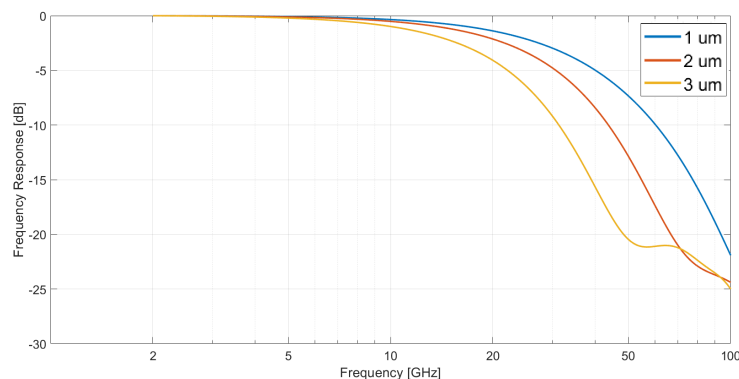


Figure 3. Frequency response of a dual depletion $\text{In}_{0.53}\text{Ga}_{0.47}\text{As}$ PIN photodiode with an active area of $500 \mu\text{m}^2$ and an absorption layer percentage of 50% , working with a 10 V applied voltage, as a function of its total length at room temperature.

In [1–3], other interesting results are reported, applying different voltages and device dimensions. However, there was no optimization process and the device was not a sensor but a photodiode in a communication system. In this article, the optimization process was performed in a temperature sensor, based on the variation in semiconductor properties with it.

4. Influence of the Structural Dimensions on the Bandwidth

This research work aimed to explore the possibility of using a dual depletion $\text{In}_{0.53}\text{Ga}_{0.47}\text{As}$ PIN photodiode as a temperature sensor. Since it was intended to verify how the photodiode bandwidth changes with temperature, it was necessary to have more details about how the response varies with the photodiode dimensions.

Various photodiode responses for an active area of $500 \mu\text{m}^2$ and a 6 V applied voltage were determined, by varying l_t and p_a . The total length l_t was in a range between $0.05 \mu\text{m}$ and $3 \mu\text{m}$; and, on the other hand, p_a varied from 0 to 1. Both varied linearly, with a total of 50 equidistant points, and all their combinations were considered.

Figure 4 shows a contour plot, where the device dimensions are varied. This problem was a multi-parameter optimization. For each combination, the device bandwidth was determined and a graph was plotted. Based on this kind of figure, it was possible to verify the best dimension combinations and determine the influence of each parameter on the frequency response.

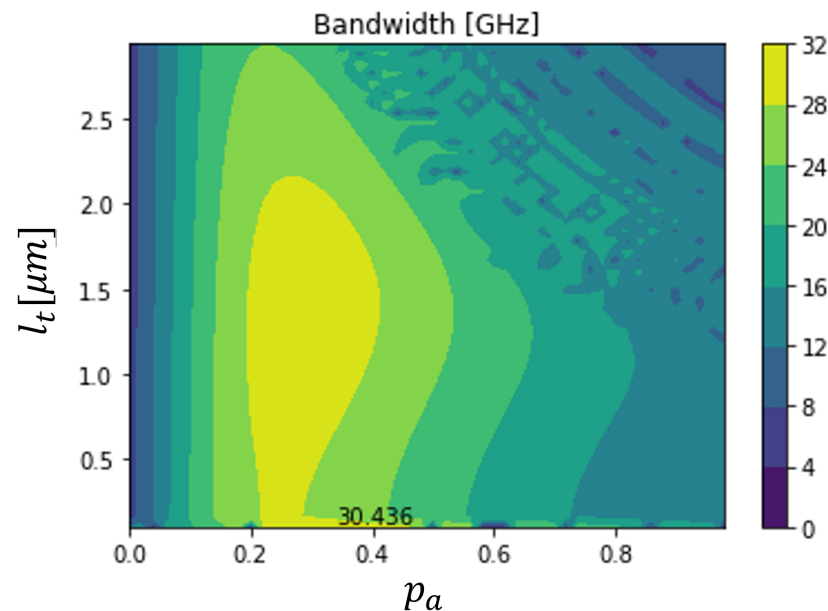


Figure 4. Bandwidth of a $500 \mu\text{m}^2$ dual depletion $\text{In}_{0.53}\text{Ga}_{0.47}\text{As}$ PIN photodiode, working with a 6 V applied voltage, as a function of its total length and its absorption layer percentage at room temperature.

The bandwidth maxima was around 30.436 GHz, with this value being within the expected range [19,10,13]. In this case, it was possible to conclude that the maximum bandwidth was higher when the absorption layer percentage was around 20% to 45% percent of the total device length. In addition, the maximum bandwidth was obtained for shorter devices, but it was also possible to obtain quite similar devices with moderate dimensions.

5. Temperature Sensor

The temperature sensor was simulated using a reference room temperature (300 K) and variations of 25 K (or 25 °C). The parameters at different analyzed temperatures are presented in Table 1. The semiconductor properties varied with temperature, a phenomena modeled using previously validated approaches from other authors, as presented in references [7,13,14].

Using this approach, one can analyze the best photodiode dimensions for obtaining the highest bandwidth variation. Thus, it is possible to obtain the temperature from this analysis. First, it is possible to perform spectral analysis, and by determining the bandwidth, estimate the temperature or, at least, verify if the temperature has varied within a certain range (in this case, verify if it was 25 K). On the other hand, it is possible to use only a certain pulse frequency. By analyzing the output power, the temperature can be determined. If that frequency is higher than the bandwidth, the output power will be at least half of the maximum power. Then, a reference (for instance, the room temperature) should be stored, and the temperature variation can be detected by the output power that is lost.

Figures 5 and 6 illustrate a rigorous sweep of both the absorption layer percentage (p_a) and total length (l_t), for a 10 V applied voltage on a $500 \mu\text{m}^2$ device. These figures allowed us to optimize the device, to verify which dimensions gave more sensitivity to temperature variations. It was concluded that there are regions where the bandwidth varies sufficiently to detect the variation, namely with absolute variations higher than 20 GHz.

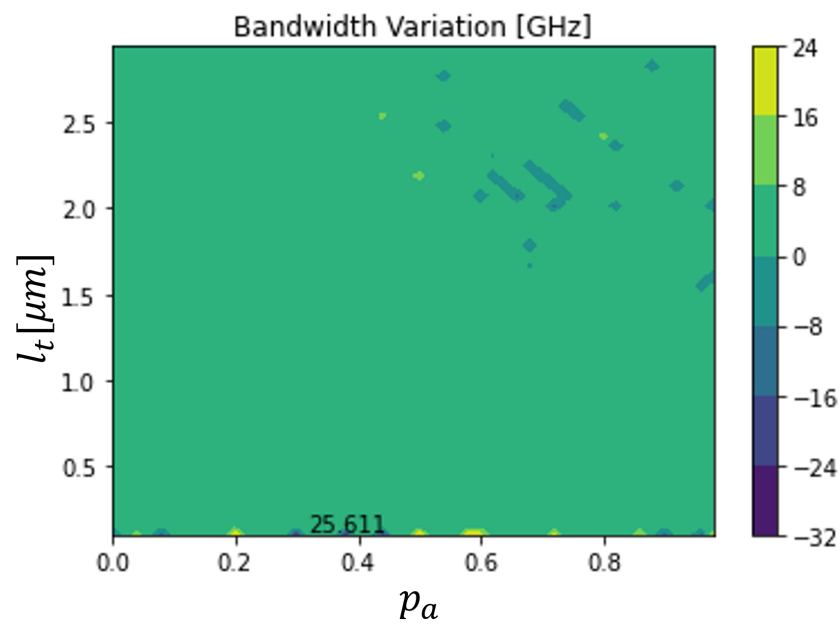


Figure 5. Bandwidth variation of a $500 \mu\text{m}^2$ dual depletion $\text{In}_{0.53}\text{Ga}_{0.47}\text{As}$ PIN photodiode, working with a 6 V applied voltage, as a function of its total length and its absorption layer percentage for a variation of -25 K .

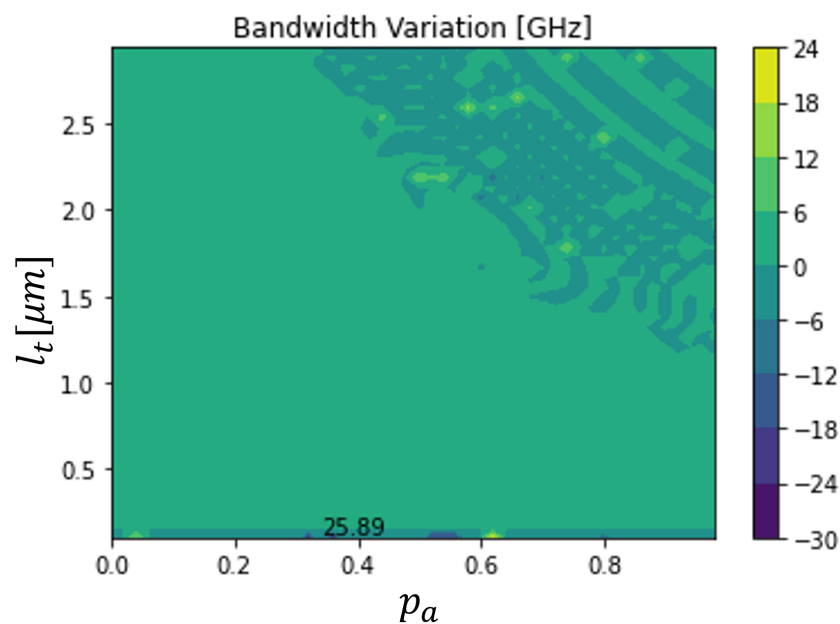


Figure 6. Bandwidth variation of a $500 \mu\text{m}^2$ dual depletion $\text{In}_{0.53}\text{Ga}_{0.47}\text{As}$ PIN photodiode, working with a 6 V applied voltage, as a function of its total length and its absorption layer percentage for a variation of $+25 \text{ K}$.

However, to detect the increase and decrease of temperature, referenced to the room temperature, the bandwidth variations have to have different signs. For that reason, the optimized temperature sensor was not the one shown in Figures 5 and 6. The maximum bandwidth variations in those conditions were -3.620 GHz and 8.374 GHz , respectively, for the temperature decrease and increase, with 10.330 GHz being the reference bandwidth. The optimized device had a total length of $2.536 \mu\text{m}$ and its absorption area was 53.95% of the total length. The obtained bandwidth variations were smaller than the maxima only for an increase or a decrease in temperature in Figures 5 and 6. However, they were sufficiently high to be detected.

6. Conclusions

The aim of this research work was to implement a method capable of modeling the frequency response of dual depletion PIN photodiodes. In addition, the device was tested as a temperature sensor, using the same approach to optimization.

The model was validated with previously published results. An $\text{In}_{0.53}\text{Ga}_{0.47}\text{As}$ was analyzed within its absorption region, namely at 1300 nm and at room temperature. The frequency response was obtained in a range from 0 to 100 GHz. The device dimensions were swept and the bandwidth was obtained at the half-power point. Then, it was possible to analyze how these parameters influenced the device's bandwidth, which was revealed to be a multiparameter optimization problem.

The semiconductors' properties were studied, in order to investigate the influence of temperature on them. To test the photodiode as a temperature sensor, two other temperature values were analyzed. By varying the semiconductor properties, the influence of temperature on the overall device response was analyzed. Bandwidths were also computed at these temperatures, which were established as 25 K variations from room temperature. By subtracting the bandwidth values at different temperatures, we could verify how this figure of merit was influenced by the temperature.

A sensor was obtained by establishing room temperature as the reference and by choosing a certain pulse frequency. For that frequency, if the output power varied -3 dB, the temperature variation was higher than the 25 K.

The device optimized for a 6 V applied voltage and an active area of $500 \mu\text{m}^2$ had a total length of $2.536 \mu\text{m}$, in which 53.95% corresponded to the absorption region. In these conditions, if the temperature increases 25 K from the room temperature, one should expect a bandwidth increase of 8.374 GHz, and if it decreases 25 K from that reference, the bandwidth should reduce by 3.620 GHz. Then, by choosing two different frequencies, it would be possible to use this device as a temperature sensor. In this case, 6.711 GHz (obtained bandwidth for 275 K) and 18.704 GHz (obtained for 325 K) should be considered.

Author Contributions: Conceptualization: R.A.M.L. and J.P.N.T.; Methodology: R.A.M.L., J.P.N.T. and C.P.C.V.B.; Software: R.A.M.L.; Validation: R.A.M.L. and J.P.N.T.; Investigation: R.A.M.L., J.P.N.T. and C.P.C.V.B. All authors have read and agreed to the published version of the manuscript.

Funding: This research received no external funding.

Institutional Review Board Statement: Not applicable.

Informed Consent Statement: Not applicable.

Data Availability Statement: Not applicable.

Acknowledgments: This work was supported in part by FCT/MCTES through national funds and in part by cofounded EU funds under Project UIDB/50008/2020. Also, this work was supported by FCT under the research grant UI/BD/151091/2021. Moreover, the authors would like to acknowledge the support of Academia Militar (AM) and Centro de Investigação, Desenvolvimento e Inovação da Academia Militar (CINAMIL) under project NA-DispOpto.

Conflicts of Interest: The authors declare no conflict of interest.

References

1. Pereira, J.M.T.; Torres, J.P.N. Frequency response optimization of dual depletion InGaAs/InP PIN photodiodes. *Photonic Sens.* **2016**, *6*, 63–70. [[CrossRef](#)]
2. Torres, J.P.; Pereira, J. Frequency Response Simulation Analysis of Waveguide Photodetectors. *Appl. Phys. Res.* **2017**, *9*, 4. [[CrossRef](#)]
3. Fernandes, C.M.C.; Pereira, J.M.T. Bandwidth modeling and optimization of PIN photodiodes. In Proceedings of the 2011 IEEE International Conference on Computer as a Tool (EUROCON), Lisbon, Portugal, 27–29 April 2011; pp. 1–4.
4. Amraoui, R.; Aissat, A.; Vilcot, J.P.; Decoster, D. Frequency response optimization of P-I-N photodiode based on InGaAsN lattice matched to GaAs for High-Speed photodetection applications. *Opt. Laser Technol.* **2022**, *145*, 107468. [[CrossRef](#)]
5. Rai, V. Temperature sensors and optical sensors. *Appl. Phys. B* **2007**, *88*, 297–303. [[CrossRef](#)]

6. Shaker, A.; Salem, M.S.; Zekry, A.; El-Banna, M.; Sayah, G.T.; Abouelatta, M. Identification of power PIN diode design parameters: Circuit and device-based simulation approach. *Ain Shams Eng. J.* **2021**, *12*, 3141–3155. [[CrossRef](#)]
7. Alizade, R.; Ghadimi, A. The study of quantum efficiency in PIN photodiodes in terms of temperature and capacitive effects under non-uniform illumination conditions. *Opt. Quantum Electron.* **2019**, *51*, 16. [[CrossRef](#)]
8. Wang, Y.; Li, G.; Gu, X.; Kong, Y.; Zheng, Y.; Shi, Y. Responsibility optimization of a high-speed InP/InGaAs photodetector with a back reflector structure. *Opt. Express* **2022**, *30*, 4919–4929. [[CrossRef](#)]
9. Malik, D.; Das, U. Design and modeling of an efficient high-speed InGaAs/InP QW waveguide-photodetector. *Opt. Quantum Electron.* **2023**, *55*, 353. [[CrossRef](#)]
10. Effenberger, F.J.; Joshi, A.M. Ultrafast, dual-depletion region, InGaAs/InP p-i-n detector. *J. Light. Technol.* **1996**, *14*, 1859–1864. [[CrossRef](#)]
11. Hammar, C.; Vinter, B. Calculation of the velocity-field characteristic of n-InP. *Solid State Commun.* **1972**, *11*, 751–754. [[CrossRef](#)]
12. Dentan, M.; Cremoux, B.D. Numerical simulation of the nonlinear response of a p-i-n photodiode under high illumination. *J. Light. Technol.* **1990**, *8*, 1137–1144. [[CrossRef](#)]
13. Verónica Matos, J.P. Numerical analysis and optimization of resonant cavity-enhanced p-i-n photodiodes. In Proceedings of the WSEAS International Multiconference on Circuits, Systems, Communications and Computers—CSCC, Lisbon, Portugal, 30 October–1 November 2014; Volume 1, pp. 62–68.
14. Jervase, H.B.J.A. Optimization procedure for the design of ultrafast, highly efficient and selective resonant cavity enhanced Schottky photodiodes. *IEEE Trans. Electron Devices* **2000**, *47*, 1158–1165. [[CrossRef](#)]

Disclaimer/Publisher’s Note: The statements, opinions and data contained in all publications are solely those of the individual author(s) and contributor(s) and not of MDPI and/or the editor(s). MDPI and/or the editor(s) disclaim responsibility for any injury to people or property resulting from any ideas, methods, instructions or products referred to in the content.